OPEN

Impact of river discharge seasonality change on tidal duration asymmetry in the Yangtze River Estuary

Xiayan Yu[1,2], Wei Zhang[1,2]* & A. J. F. Hoitink[3]

The Yangtze River Estuary (YRE) is one of the world's largest river-tidal systems with rapidly changing hydrology and morphology following the construction of multiple dams. The effects of dam construction may extend to the region close to the coast, where channel stability depends on the asymmetry of the tide. Here, we focus on the possible effects of changing discharge regimes on tidal asymmetry in the YRE. Specifically, we focus on the difference in duration between ebb and flood, quantified as tidal duration asymmetry, because it has strong implications for residual sediment transport and can be derived from available water level data. To cope with nonstationary tides under the influence of a time-varying river discharge, a nonstationary harmonic analysis tool (NS_TIDE) is applied to explore the spatiotemporal variations in tidal duration asymmetry, under the influence of different combinations of tidal constituents. Tidal duration asymmetry initially increases, then slightly decreases, in an upstream direction. It experiences significant seasonal variations in response to rapidly varying discharge: tides are more asymmetric upstream of Zhenjiang in the dry season and more asymmetric downstream in the wet season. The combined effects of discharge regulation and morphological changes cause seasonal alterations in tidal duration asymmetry. In the wet season, reduced river discharge caused by water storage and climate change enhance the asymmetry upstream (+11.74% at Wuhu, +7.19 at Nanjing) while the asymmetry is weakened downstream (−2.90% at Zhenjiang, −7.19 at Jiangyin) following the TGD's operation. Downstream channel erosion caused by post-TGD lower sediment loads has become the dominant factor weakening tidal asymmetry in most parts of the YRE in the dry season. Understanding these evolutions of tidal duration asymmetry under the hydrological and morphological effects has important implications for the management of estuarine ecosystem and navigation.

Dams are built for various purposes, such as irrigation, flood control and power generation[1]. The various impacts of dams have been subject to study and debated for decades. The changes in river and sediment discharges due to dam constructions have long been recognized as far-reaching[2–4]. Dams play an important role in eliminating peak river discharge and stabilizing low river discharge[5]. Beyond discharge regulation, dams also lead to a drop in sediment loads, thereby impacting estuarine morphology[4,6–9], which is crucially dependent on tidal asymmetry[10,11]. Here, we focus on tidal duration asymmetry, which quantifies the periodic difference between the durations of falling and rising tidal water level[12,13]. Tidal duration asymmetry characterizes flood and ebb dominance[14–16], and can directly be derived from long-term water level data.

Tidal asymmetry can be produced when tides propagate into shallow-water areas, where tidal distortion results in rising high-frequency harmonic constituents[14,17]. The physical mechanisms responsible for tidal duration asymmetry are represented by the nonlinear effects related to tidal interactions among constituents and irregular estuarine topography[13,14,18,19]. Tides can be strongly modulated by river flow and have a complex behavior in estuaries[20,21]. Rapidly varying river discharges can generate significant nonstationary features[22–24],

[1]State Key Laboratory of Hydrology-Water Resources and Hydraulic Engineering, Hohai University, Nanjing, 210098, China. [2]College of Harbor, Coastal and Offshore Engineering, Hohai University, Nanjing, 210098, China. [3]Hydrology and Quantitative Water Management Group, Wageningen University & Research, Droevendaalsesteeg 3, 6708, Wageningen, The Netherlands. *email: w.zhang@hhu.edu.cn

characterized by tidal attenuation and tidal energy transfer between tidal frequencies as a frictional effect[25–29]. Thus, tide-river interactions can significantly influence tidal duration asymmetry[23]. When tidal elevation and velocity are near quadrature, the tidal duration asymmetry can be related to flow velocity asymmetry[12,30,31], which has an important influence on sediment transport[17,32–34]. Tidal duration asymmetry also plays an important role in navigation and ecosystems by affecting the fluctuations in water levels and bed friction[22].

It is common practice to evaluate tidal asymmetry by the harmonics of astronomical tides using the amplitude ratio between the semidiurnal tide M_2 and its first harmonics M_4 (M_4/M_2) to quantify the degree of distortion[15]; the phase difference ($2M_2 - M_4$) is used as a metric to reflect the direction of tidal asymmetry[12–14,32,34,35]. This approach can be extended to evaluate the contributions of triad combinations of tidal constituents, such as $K_1/O_1/M_2$, which is important in mixed tidal regimes[18,19]. Song et al.[36] followed the approach taken by Nidzieko[31] and generalized the skewness metric to determine the contributions of different tidal interactions, where the tidal combinations have a frequency relationship of $2\omega_1 = \omega_2$ for pairs or $\omega_1 + \omega_2 = \omega_3$ for triads, such as $K_1/O_1/M_2$.

China's Yangtze River Estuary (YRE) is a natural system whose hydrodynamics exhibit strong spatiotemporal variations, making it an excellent location to investigate estuarine tidal dynamics. Although the characteristics of tidal propagation in the YRE have been widely studied[37,38], the effects of river discharge have long been neglected and remain a challenge to understand nonstationary tidal dynamics. Recently, increasing attention has been paid to the responses of tidal dynamics to varying river discharge in the YRE[23,39–44], but few of those have described the long-term evolutions of tidal properties. In particular, it is of interest to establish the contrast before and after the operation of the Three Gorges Dam (TGD), which is the world's largest river damming project. Its impacts have raised public concern following rapid economic development and increasing awareness of possible negative impacts for natural resources and the environment[45–47].

Previous studies have focused on water discharge[48,49], sediment load[50–52], estuarine Suspended Sediment Concentration[53], delta evolution[4,45,54,55] and sediment grain size[56–58]. To mitigate floods and droughts in the middle and lower regions of the Yangtze River, the TGD reduces the peak discharge in the wet season whereas increases discharge during the dry season[48,49,59]. The riverine sediments are mostly trapped in reservoirs, causing severe channel erosion in the subaqueous delta[4,60,61]. These seasonal discharge regulation and morphological changes significantly affect the tidal dynamics in the YRE. Little is known about the impact of the dam on estuarine tidal dynamics. Zhang et al.[62] used a numerical model to study the interactions between tidal waves and river discharge with reference to the TGD's impact focusing on different tidal constituents. The dominant M_2 tide has decreased from the dry season to wet season. Cai et al.[63] investigated the effects of the TGD on spatiotemporal variations in tide-river dynamics, with the largest change occurring in autumn. In addition, the YRE has undergone significant morphological changes under the influences of human activities such as dam constructions and land use patterns[45,56,61,64,65], which also affect the tidal duration asymmetry in the system. Hence, a better understanding of the relationship between tidal duration asymmetry and river discharge and morphology with respect to the TGD is still missing.

In this study, the changes in tidal duration asymmetry due to different tidal combinations are investigated in the YRE with respect to the large and strongly variable river discharge and morphological changes related to the effects of the TGD. A nonstationary harmonic model (NS_TIDE) is applied to long-term observational data in the YRE to assess the spatiotemporal variations in the tidal duration asymmetry in the pre- and post-TGD periods. The seasonal evolution of tidal duration asymmetry may inform other tidal estuaries under the impact of large dams, thus providing a basis for further understanding these dynamics elsewhere in the world.

Methods

Study area.
The Yangtze River, with a drainage area of 1.8×10^6 km^2, is the largest river in southern Asia[4]. The YRE is located on the eastern China coast. As the major channel connecting the Yangtze River and East China Sea, the YRE is influenced by moderate tides and strongly varying river discharges[66]. The YRE has a semidiurnal tidal regime (($a_{K_1} + a_{O_1}$)/($a_{M_2} + a_{S_2}$) < 0.25, in which a represents tidal amplitude), where M_2 is the dominant tide and followed by S_2, K_1 and O_1. Under the intermediate river flow and tidal conditions, Jiangyin is the landward limits of tidal current reversal (240 km away from the mouth), while the tidal wave propagates upstream until Datong (645 km away from the mouth).

The YRE has an annual mean river discharge of approximately 27,500 m^3/s at Datong for the whole study period (1965–1985 & 2003–2014). However, seasonal discharge varies substantially under the influence of the summer Asian monsoon, with low discharge during the dry season (November to April) and high discharge during the wet season (May and October) (Fig. 1). In addition, river discharge at Datong experiences a significant seasonal regulation after the operation of the TGD, characterized by a decrease of 3430 m^3/s (altered from 39611 m^3/s to 36181 m^3/s) during the wet season and a slight increase of 231 m^3/s (altered from 16210 m^3/s to 16441 m^3/s) during the dry season (Fig. 1). Those changes can be attributed to the combined effects of the TGD regulation and climate changes that have occurred in the Yangtze basin[67,68].

Data overview.
The YRE, as a subject of our analysis, has been intensively monitored for water levels since the mid-1950s. Available hydrological data were divided into 2 periods according to the TGD operation in 2003: the pre-TGD period (1965–1985, before the impoundment of the TGD) and the post-TGD period (2003–2014, after the operation of TGD). The period 1986–2002 was not included in our analysis due to lack of data. Water level data spanning the two periods at six hydrological stations which are located throughout the estuary were collected. The location of these stations in the YRE are presented in Fig. 2 and the data periods of all stations are listed in Table 1. Water level data of six stations were adjusted to Wusong mean sea level for the analysis. For the purpose of harmonic analysis, the original high-low water level data are interpolated into one-hour intervals (Appendix A). In addition, a series of daily-averaged river discharge data for the pre and post periods at Datong
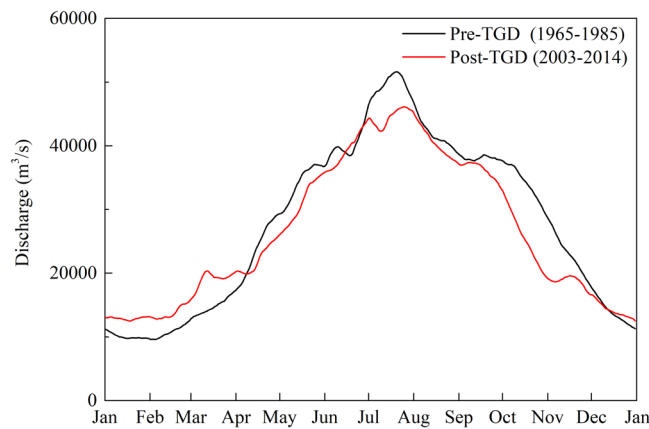
Figure 1. Yangtze River discharge at the Datong gauging station before and after the operation of the TGD.
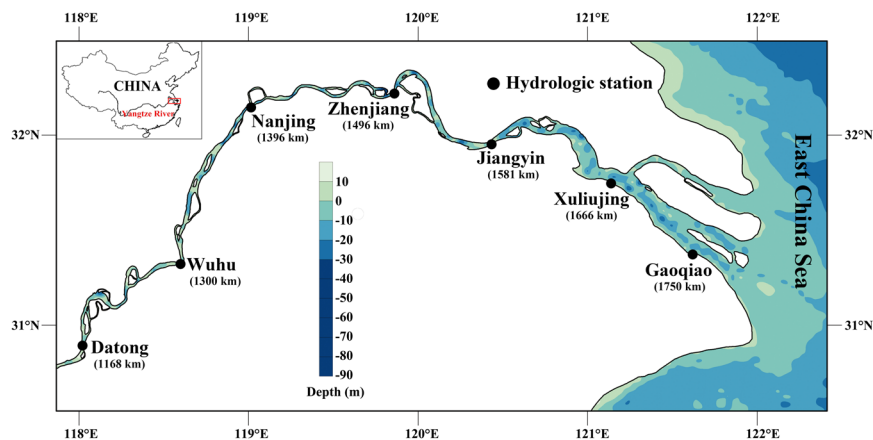

Figure 2. Map of the Yangtze River Estuary and the locations of hydrological stations. The numbers in brackets are distance downward the Three Gorges Dam. Note: the maps were created using Surfer 13 (www. goldensoftware.com/products/surfer).

are used to establish the impact of river discharge. All the data are collected from the Hydrological Yearbooks of the People's Republic of China, published by the Yangtze Hydrology Bureau of China.

Methodology. *Nonstationary harmonic analysis method.* Harmonic analysis (HA), which determines tidal amplitudes and phases by a least squares regression analysis, traditionally assumes that tides are perfectly stationary[69,70]. However, tides in estuaries are affected not only by astronomical tidal forcing but also nonlinear interactions generating subharmonics (e.g. river flow, channel geometry and friction)[71]. The traditional HA is not effective enough for the analysis of river tides when the river flow is strongly variable. A nonstationary harmonic analysis method (NS_TIDE) is developed based on T_TIDE[72] by embedding the nonstationary forcing into the tidal basis functions[73]. It has been applied to the Columbia River Estuary[73] and St. Lawrence River[74] to prove that it can be a useful method in analyzing the nonstationary water level record reflected by external forcing (oceanic tide and river flow) and nonlinear interactions. NS_TIDE can effectively distinguish frequencies within tidal bands without sacrificing resolution in the time domain or data at the end of time series.

The NS_TIDE method developed by Matte *et al.*[73,74] is applied to estimate spatial and temporal evolutions of tidal harmonic constants. In this nonstationary tidal harmonic model, the total tidal height is given as:

$$
\begin{aligned}
h(t) = c_0 + c_1 Q^{p_s}(t - t_Q) + c_2 \frac{R^{q_s}(t - t_R)}{Q^{r_s}(t - t_Q)} \\
+ \sum_{k=1}^{n} \left[\left(d_{0,k}^{(c)} + d_{1,k}^{(c)} Q^{p_f}(t - t_Q) + d_{2,k}^{(c)} \frac{R^{q_f}(t - t_R)}{Q^{r_f}(t - t_Q)} \right) \cos(t) \right. \\
\left. + \left(d_{0,k}^{(s)} + d_{1,k}^{(s)} Q^{p_f}(t - t_Q) + d_{2,k}^{(c)} \frac{R^{q_f}(t - t_R)}{Q^{r_f}(t - t_Q)} \right) \sin(t) \right]
\end{aligned}
\tag{1}
$$

No.	Station name	Location		Data period	Distance to TGD (km)
		Longitude (E)	Latitude (N)		
1	Datong	117°38′	30°46′	1965–1985, 2003–2014	1115
2	Wuhu	118°21′	31°21′	1965–1985, 2003–2014	1239
3	Nanjing	118°43′	32°05′	1965–1985, 2003–2014	1335
4	Zhenjiang	119°26′	32°13′	1965–1985, 2003–2014	1435
5	Jiangyin	120°18′	31°57′	1965–1985, 2003–2014	1520
6	Xuliujing	120°57′	31°46′	1982–1985, 2003–2014	1605
7	Gaoqiao	121°33′	31°23′	1965–1985, 2003–2014	1685

Table 1. Location of hydrological stations and the corresponding periods of valid data.

where c_0, c_1 and c_2 denote the coefficients of stage model; Q represents the upstream river flow; R represents the greater diurnal tidal range at the reference station; p_s, q_s, r_s, p_f, q_f and r_f are the exponents for each station and frequency band, which are obtained by an iterative procedure, where the subscripts s and f refer to the stage and tidal-fluvial models, respectively; $d_{0,k}$, $d_{1,k}$ and $d_{2,k}$ are the model coefficients for the tidal-fluvial model, while the superscripts c and s denote the cosine and sine terms; t_Q and t_R are the time-lags capturing the average propagation time of waves to the station, determined by calculating the maximum correlation between Q or R time series and the observed data.

Model performance.   The 'harmonic constants' are not constant over time in the YRE, where the river flow is strongly variable and the tidal signal is highly nonstationary. Hence, the observations at Wuhu in 2014 with hindcasts obtained by the NS_TIDE and T_TIDE models are compared to evaluate the effectiveness and applicability of NS_TIDE in the YRE (Fig. 3a). T_TIDE is unable to resolve seasonal fluctuations related to variable river discharge, while NS_TIDE is far more accurate, especially during the wet season (Fig. 3b). The root-mean-square errors (RMSE) values are calculated at six gauging stations (Fig. 3c). The RMSE for both models are comparable at downstream stations, while the RMSE for T_TIDE increase sharply upstream under the significant influence of river discharge. For T_TIDE, the hindcast explains 86.44% of the original signal variance and has a RMSE of 0.710 m at Wuhu. Results from NS_TIDE sharply improves compared to T_TIDE: the hindcast explains 99.64% of the original signal variance and has an RMSE of 0.146 m. Thus, NS_TIDE is applied to further analyses in this study.

Tidal skewness metric.   The skewness metric is used in the present study to analyze the characteristics of overall tidal duration asymmetry and to determine the contributions of different combinations of tidal constituents. This metric depends on the tidal amplitudes (a) and phases (φ), as well as frequencies of tidal constituent (ω). As indicated in Song et al.[36], the skewness is obtained as:

$$\gamma_2 = \frac{\frac{3}{4}a_1^2\omega_1^2 a_2\omega_2 \sin\left(2\varphi_1 - \varphi_2\right)}{\left[\frac{1}{2}\left(a_1^2\omega_1^2 + a_2^2\omega_2^2\right)\right]^{3/2}}$$ (2)

and

$$\gamma_3 = \frac{\frac{3}{2}a_1\omega_1 a_2\omega_2 a_3\omega_3 \sin\left(\varphi_1 + \varphi_2 - \varphi_3\right)}{\left[\frac{1}{2}\left(a_1^2\omega_1^2 + a_2^2\omega_2^2 + a_3^2\omega_3^2\right)\right]^{3/2}}$$ (3)

where $2\omega_1 = \omega_2$ (pairs) in Eq. (2) and $\omega_1 + \omega_2 = \omega_3$ (triads) in Eq. (3), respectively. The contribution of different combinations of two or three tidal constituents to total tidal skewness is calculated as follows:

$$\beta_2 = \frac{\frac{3}{4}a_1^2\omega_1^2 a_2\omega_2 \sin\left(2\varphi_1 - \varphi_2\right)}{\left(\frac{1}{2}\sum_{i=1}^{N}a_i^2\omega_i^2\right)^{3/2}} = \gamma_2 \cdot \left(\frac{a_1^2\omega_1^2 + a_2^2\omega_2^2}{\sum_{i=1}^{N}a_i^2\omega_i^2}\right)^{3/2}$$ (4)

for pairs or

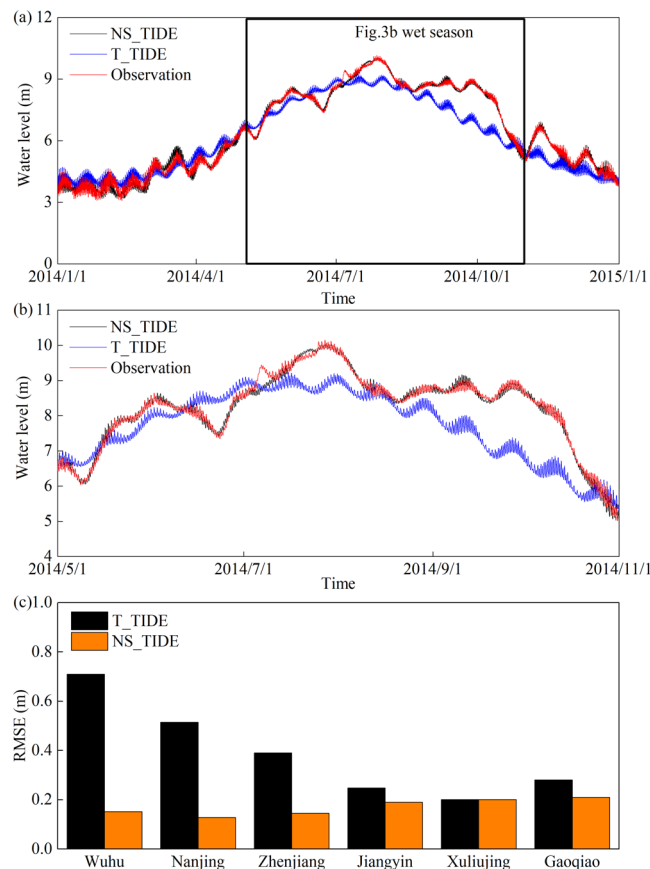**Figure 3.** (**a**) Comparison of observed water level at Wuhu in 2014 with hindcasts obtained from the NS_TIDE and T_TIDE models; (**b**) zoom-in of data in wet season; (**c**) Root-mean-square error (RMSE) of water level hindcasts at 6 hydrological stations ordered from upstream to downstream.

$$\beta_3 = \frac{\frac{3}{2}a_1\omega_1 a_2\omega_2 a_3\omega_3 \sin\left(\varphi_1 + \varphi_2 - \varphi_3\right)}{\left(\frac{1}{2}\sum_{i=1}^{N}a_i^2\omega_i^2\right)^{3/2}} = \gamma_3 \cdot \left(\frac{a_1^2\omega_1^2 + a_2^2\omega_2^2 + a_3^2\omega_3^2}{\sum_{i=1}^{N}a_i^2\omega_i^2}\right)^{3/2} \tag{5}$$

for triplets. Thus, the total tidal skewness is calculated as the summation of the individual β.

$$\gamma_N = \sum\beta_2 + \sum\beta_3 \tag{6}$$

The sign of tidal skewness reflects the direction of tidal duration asymmetry and the value can reflect the degree of distortion. For $\gamma_N < 0$, the falling tide duration is shorter than the rising tide duration. Conversely, the positive value for tidal skewness ($\gamma_N > 0$) indicates shorter rising tide duration.

Relative sensitivity coefficient (RSC). The tidal skewness evaluates the contributions of each combination to tidal duration asymmetry based on the amplitudes, phases and frequencies of the constituents. The non-dimensional relative sensitivity coefficient (RSC)[75] is introduced to study the sensitivity of tidal skewness contributed by different tidal combinations to the attenuation of the corresponding tidal amplitude. The expression of the RSC reads:

$$S_a = \lim_{\Delta A \to 0}\left(\frac{\Delta\gamma/\gamma}{\Delta a/a}\right) = \frac{\partial\gamma}{\partial a} \cdot \frac{a}{\gamma} \tag{7}$$

Generally, the RSCs for combination of two or three constituents are obtained as follows:

$$S_{a_1} = \frac{\partial\gamma}{\partial a_1} \cdot \frac{a_1}{\gamma} = \frac{2a_2^2\omega_2^2 - a_1^2\omega_1^2}{a_1^2\omega_1^2 + a_2^2\omega_2^2} \tag{8}$$

$$S_{a_2} = \frac{\partial\gamma}{\partial a_2} \cdot \frac{a_2}{\gamma} = \frac{a_1^2\omega_1^2 - 2a_2^2\omega_2^2}{a_1^2\omega_1^2 + a_2^2\omega_2^2} \tag{9}$$

	K$_1$		O$_1$		M$_2$		S$_2$		M$_4$		MS$_4$		M$_6$		
	a(m)	p(°)	a(m)	p(°)	a(m)	p(°)	a(m)	p(°)	a(m)	p(°)	a(m)	p(°)	a(m)	p(°)	K
Wuhu	0.043	75	0.037	40	0.111	47	0.041	103	0.020	360	0.018	41	0.005	300	0.522
Nanjing	0.079	29	0.063	330	0.243	324	0.084	26	0.042	200	0.038	245	0.011	78	0.432
Zhenjiang	0.119	354	0.092	293	0.433	261	0.130	320	0.084	73	0.075	122	0.022	245	0.376
Jiangyin	0.173	295	0.121	237	0.769	160	0.236	220	0.137	234	0.127	281	0.035	307	0.293
Xuliujing	0.207	253	0.142	199	0.924	86	0.250	145	0.149	91	0.136	133	0.028	81	0.298
Gaoqiao	0.244	215	0.162	157	1.118	16	0.285	14	0.123	308	0.106	349	0.020	241	0.289

Table 2. Tidal amplitudes (a) and phases (p) of main constituents in the YRE.

for the combination of two constituents, and

$$S_{a_1} = \frac{\partial \gamma}{\partial a_1} \cdot \frac{a_1}{\gamma} = \frac{a_2^2 \omega_2^2 + a_3^2 \omega_3^2 - 2a_1^2 \omega_1^2}{a_1^2 \omega_1^2 + a_2^2 \omega_2^2 + a_3^2 \omega_3^2} \tag{10}$$

$$S_{a_2} = \frac{\partial \gamma}{\partial a_2} \cdot \frac{a_2}{\gamma} = \frac{a_1^2 \omega_1^2 + a_3^2 \omega_3^2 - 2a_2^2 \omega_2^2}{a_1^2 \omega_1^2 + a_2^2 \omega_2^2 + a_3^2 \omega_3^2} \tag{11}$$

$$S_{a_3} = \frac{\partial \gamma}{\partial a_3} \cdot \frac{a_3}{\gamma} = \frac{a_1^2 \omega_1^2 + a_2^2 \omega_2^2 - 2a_3^2 \omega_3^2}{a_1^2 \omega_1^2 + a_2^2 \omega_2^2 + a_3^2 \omega_3^2} \tag{12}$$

for the combination of three constituents, where a_1, a_2 and a_3 refer to tidal amplitude, ω_1, ω_2 and ω_3 are the tidal frequencies. The positive/negative values of RSCs typically suggest the positive/negative correlation between tidal skewness and amplitudes. Specifically, an S_a value of 0.5 indicates that a 10% decrease of the tidal amplitude a can make the corresponding tidal skewness (γ) decrease by 5%. A larger absolute value of the coefficient (RSC) is interpreted as a more significant effect of the variable A on the corresponding tidal duration asymmetry.

Results

Spatial patterns of tidal dynamics. *Spatial patterns of tidal amplitudes and phases.* The spatial variations in the amplitudes and phases of the seven main tidal constituents (K$_1$, O$_1$, M$_2$, S$_2$, M$_4$, MS$_4$ and M$_6$) at the six hydrological stations modelled by NS_TIDE are presented in Table 2. The diurnal (K$_1$ and O$_1$) and semi-diurnal (M$_2$ and S$_2$) constituents show a landward decrease and the amplitudes are maximum at the most seaward station (Gaoqiao). The amplitudes of K$_1$ and O$_1$ are in the range of 0.04–0.24 m and 0.04–0.16 m, respectively. As the dominant constituent in the YRE, M$_2$ is larger than other constituents with an amplitude ranging from 0.11–1.12 m. The S$_2$ amplitude is 0.04–0.29 m, about 1/4-1/3 of the M$_2$ amplitude. According to Godin[28], the decay of tidal amplitudes is frequency-dependent: the tidal constituents with lower frequencies decay more slowly than those with higher frequencies. The development of tidal phases also seems to agree with this trend.

When tides propagate into the YRE, they are significantly distorted, as expressed in the generation of shallow-water constituents, such as M$_4$, MS$_4$ and M$_6$. This distortion is characterized by an initial increase and subsequent rapid decrease of shallow water tidal amplitudes further upstream. M$_4$ varies similarly to MS$_4$, likely due to their close frequencies. The amplitudes of M$_4$ and MS$_4$ increase toward the lower reaches of the estuary, peaking at 0.15 m and 0.14 m, respectively. These two quarter-diurnal constituents are suppressed at Xuliujing, where frictional damping gradually becomes dominant over shallow-water amplification. Similar patterns are noted for M$_6$, with a peak amplitude of 0.04 m at Jiangyin.

The character of the tides can be quantified by the tidal form number *F*, expressed as $F = \frac{K_1 + O_1}{M_2 + S_2}$[76,77]. It varies in the range of 0.289–0.522 for the YRE, indicating that the YRE can be classified as a mixed semidiurnal tidal regime (0.25 < *F* < 1.5). The tidal form number generally show an increasing trend when the tidal wave propagates upstream, possibly because the semidiurnal constituents fade out faster than the diurnal constituents (which have higher frequencies).

Spatial pattern of the overall tidal duration asymmetry. The tidal skewness (β) offers a concise and quantitative way to describe the overall tidal duration asymmetry. Four major tidal combinations are selected for this purpose (Fig. 4). Tidal duration asymmetry originating from the interactions of both astronomical tides and shallow-water constituents in the YRE is predominantly flood dominant, as reflected by the positive values of β at the six stations. The overall flood asymmetry has a significant landward increase and is followed by a slight decrease upstream.

Generally, nonlinear tidal interactions are the main drivers of tidal duration asymmetry within the YRE, of which M$_2$/M$_4$ is the most important contributor with the largest magnitude (Fig. 4), followed by M$_2$/S$_2$/MS$_4$, which accounts for ~30% of the total tidal skewness. M$_2$/M$_4$/M$_6$ ranks third. Overall, the asymmetry induced by these nonlinear effects first increases and then decreases, in line with the spatial evolution of the overall tidal duration asymmetry. In comparison, the K$_1$/O$_1$/M$_2$ triad has a relatively small skewness value and retain a slight increase from the lower reaches to the tidal river. This indicates that the tide entering the channel is flood-dominant
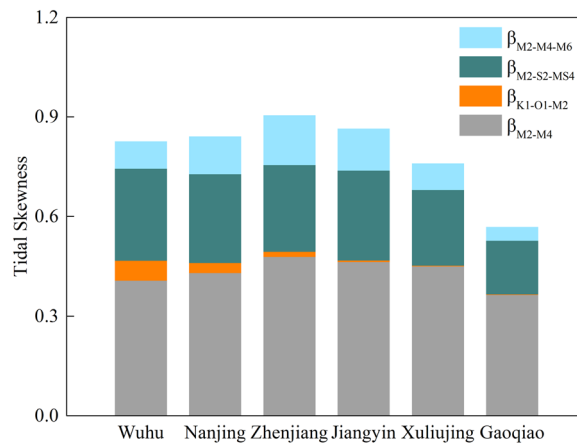
Figure 4. Total tidal skewness (β) contribution from the four major constituent combinations for each of the six hydrological stations.

within the YRE. However, $K_1/O_1/M_2$ in the YRE behaves differently from other tidal systems, such as the southern California coast[31,78] and the Pearl River Delta[16], where tidal duration asymmetry is ebb-dominant prior to non-linear tidal distortions within the tidal systems. This difference may be related to channel geometrical properties and the interactions between tidal constituents[31].

Seasonal variations in tidal dynamics.   *Seasonal variations in tidal amplitudes and phases.*   The variations in tidal amplitudes and phases at the six gauging stations are shown in Fig. 5 for the wet season and the dry season. The astronomical tidal constituents show significant seasonal variations. Smaller amplitudes are found upstream in the wet season, likely due to the higher river discharge that attenuate astronomical tides via friction. In addition, the seasonal differences in astronomical tidal amplitudes are more significant upstream than in the middle part of the YRE, showing a pattern opposite to that observed in the lower reaches of the YRE, where increasing discharge raises the water level and increased the tidal amplitude[74]. The trends in the tidal phase reflect the speed of tidal propagation along the river. Increasing river discharge delays the tidal propagation, leading to an increase in the astronomical tidal phase in the wet season at the upstream stations. In the lower reaches of the YRE, smaller astronomical tidal phases occur in the wet season due to deeper water as the river discharge increases[74].

As for the shallow-water constituents, the high river discharge during the wet season increases the tidal amplitudes in the downstream region by enhancing the nonlinear effect and stimulating tidal energy transfer from astronomical tides to shallow-water tides (Fig. 5). As tides propagate to the upper reach of the YRE, smaller tidal amplitudes occur in the wet season, when higher river discharge leads to a more significant tidal damping process by enhancing the frictional effects. The variations in shallow-water constituent phases show similar characteristics as the astronomical constituents on a seasonal scale: they increase because of larger discharge in the wet season, especially at the upstream stations.

Seasonal variations in tidal duration asymmetry.   Tidal skewness displays significant seasonality variations (Fig. 6). In the upper reaches, tidal duration asymmetry in the dry season is more significant than in the wet season. In addition, a significant difference ($\gamma_{dry\ season} - \gamma_{wet\ season} = 0.111$, corresponding to 14.67%) occurs at Wuhu, while a slight difference ($\gamma_{dry\ season} - \gamma_{wet\ season} = 0.013$, corresponding to 1.46%) occurs at Zhenjiang, which suggests that the effects of river discharge are more significant upstream. However, the opposite pattern occurs at the downstream stations, except at Gaoqiao. This may reflect the enhanced effects of nonlinearities due to increasing discharge during the wet season[41,79,80], leading to stronger shallow-water tides and weaker astronomical tides. The generation of forced constituents and the decay of basic constituents are the major factors influencing the generation of tidal duration asymmetry in the YRE, such that flood asymmetry is enhanced at the downstream stations in the wet season. Around the estuary mouth, the effects of discharge are less significant, making the seasonal variations least obvious at Gaoqiao.

Changes in the tidal duration asymmetry between the pre- and post-TGD periods.   To estimate the impacts of the TGD on the tidal dynamics in the YRE, the differences between the pre-YGD and post-TGD periods are evaluated in Fig. 7 ($\Delta_a = a_{post-TGD} - a_{pre-TGD}$ and $\Delta_p = p_{post-TGD} - p_{pre-TGD}$, where a and p refer to the tidal amplitude and phase, respectively). During the wet season, the values of Δ_a for the astronomical tides (K_1, O_1, M_2 and S_2) at most stations are positive because of the significant decrease in the river discharge caused by water storage (Fig. 7a). Similarly, shallow-water tidal amplitudes increase at the upstream stations after the TGD's operation (Fig. 7b). The strength of amplitude increase varies significantly along the channel, with the smallest Δ_a occurring at the most seaside station (Gaoqiao) because the impacts of river discharge are smallest at the mouth of the estuary. However, the largest differences do not necessarily occur in the upper reaches due to the significant attenuation over longer distances. Consequently, Jiangyin (in the middle reach) displays the most
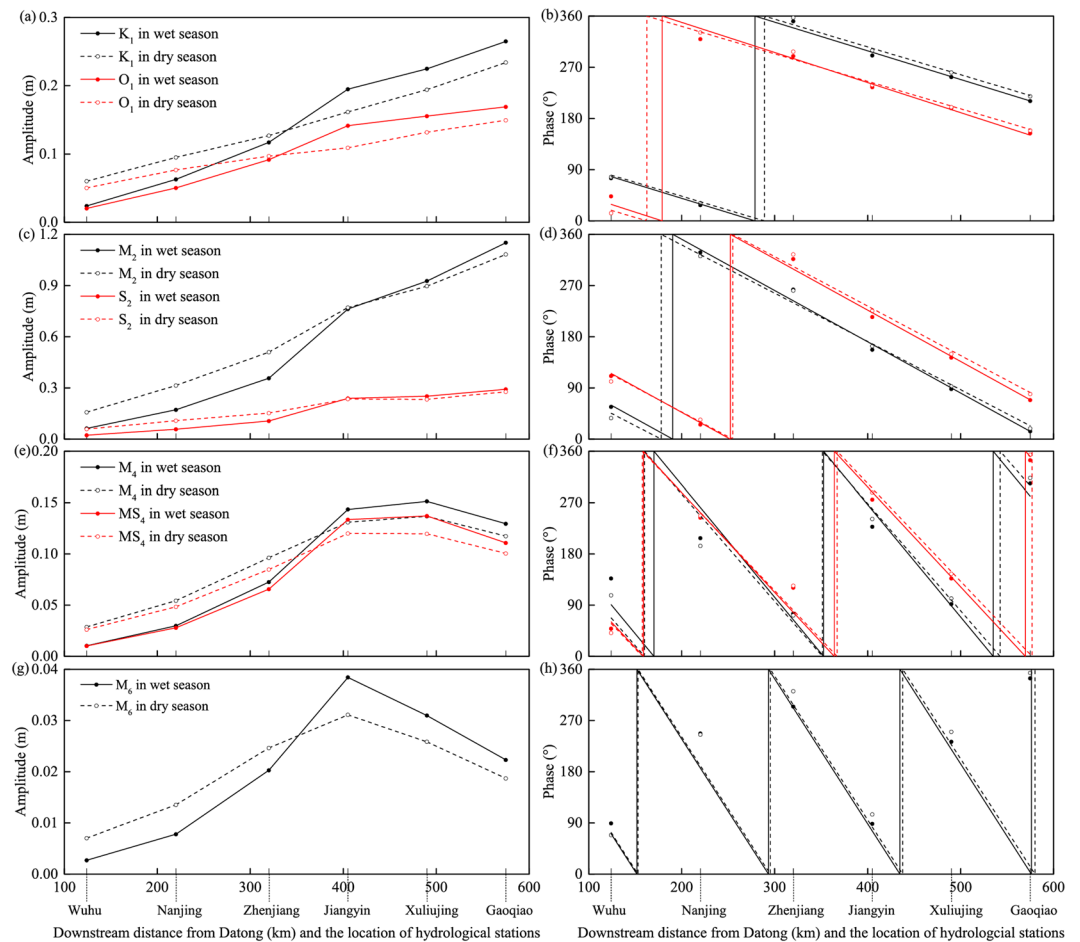
Figure 5. Seasonal dynamics of tidal amplitude and phase for (**a–d**) the main astronomical (K_1, O_1, M_2 and S_2) and (**e–h**) shallow-water constituents (M_4, MS_4 and M_6) at six hydrological stations.
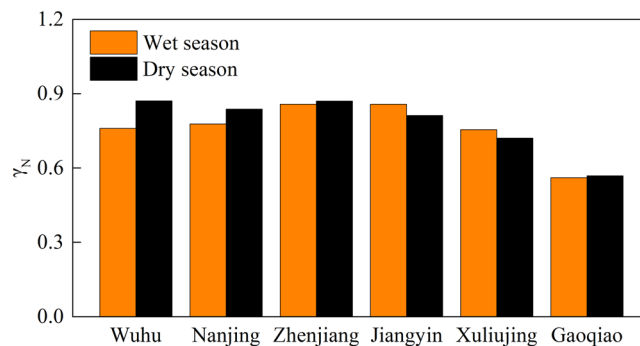

Figure 6. Comparison of tidal skewness during the flood and dry season for the six hydrological stations.

significant amplitude variations under the effects of the regulated river discharge. This is consistent with Zhang et al.[62], in which the numerical modelling shows that the largest differences occur in the middle part of the YRE. The speed of tidal propagation can be seen in variations of tidal phases. As for the changes in tidal phases during the wet season, reduced river discharge allows tides to propagate further into the YRE, characterized by smaller tidal phases in the post-TGD period, especially for the tidal constituents with higher frequencies. With increased river discharge, the largest decrease in tidal phases occurs at Wuhu.

The YRE experienced not only discharge regulation but also the morphological changes. The impact of morphological changes on tidal dynamics gradually becomes dominant in the dry season, when discharge regulation is insignificant. It can be seen from Fig. 1 that river discharge increases by only 231 m³/s (corresponding to 1.4%) after the operation of the TGD. Hence, an understanding of the morphological impacts on tidal dynamics becomes increasingly important. The TGD's operation lead to a dramatic reduction in sediment supply in the
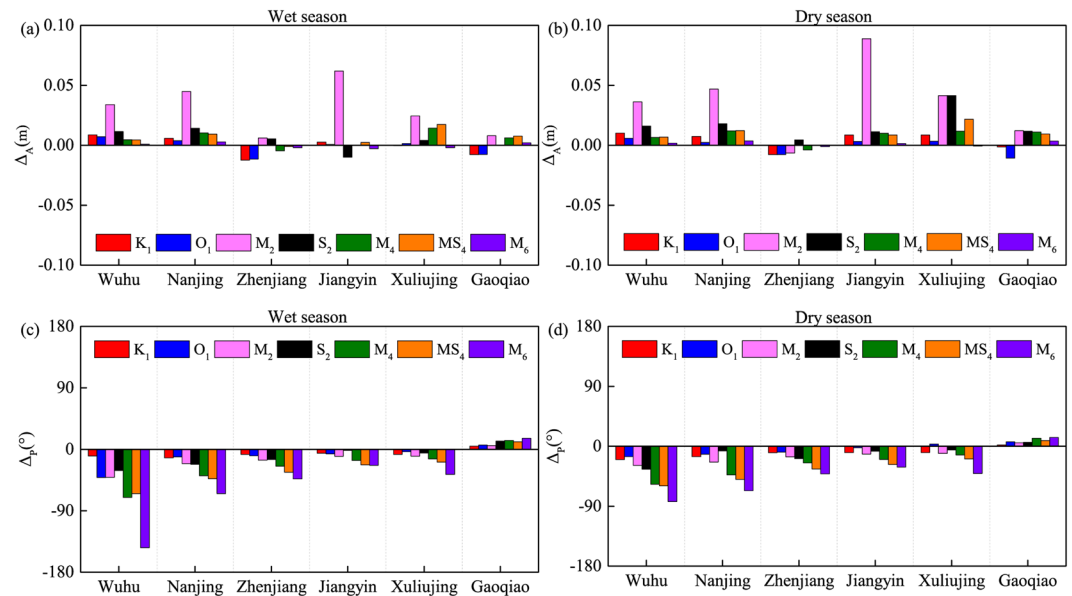
Figure 7. Differences in tidal amplitudes and phases for all six hydrological stations in the wet (**a,c**) and dry (**b,d**) season before and after TGD's operation.

YRE[56], increasing erosion[61] and causing channel deepening, which reduces bottom friction[79,81,82]. It reduces tidal attenuation along the channel[41], resulting in increased tidal amplitudes at most stations after the TGD's operation (Fig. 7c). The deepening channel also makes it easier for the tides to enter the estuary, as reflected by the decreased tidal phase (Fig. 7d). A weakened friction caused by channel deepening causes the tides to propagate faster into the estuary after the operation of the TGD. Because of the intense attenuation effects of high river discharge, the tidal amplitudes in the wet season are smaller than in the dry season, so that the amplitude change is insignificant. As a result, the amplitude differences are relatively small in the wet season. Changes in the tidal phase during the wet season are more significant under the combined effects of discharge regulation and morphological changes.

During the wet season, the post-TGD tidal skewness increases (compared to pre-TGD values) in the upper reaches at Wuhu (0.081) and Nanjing (0.057), but decreases in the middle reaches. These obvious seasonal differences are largely due to reduced river discharge caused by water storage. The difference between the two periods is negligible at Xuliujing, indicating that the impact of the discharge regulation weakens with the distance from the TGD. Tidal skewness also varies significantly in the dry season (see red columns in Fig. 8). The tidal duration asymmetry is slightly weakened in the upper and middle reaches after the TGD's operation in response to increasing channel depth, similar to the Pearl River Delta[16] and the Ems Estuary[83]. The frictional effects are reduced with increasing water depth, which weakens tidal attenuation along the channel. Since the attenuation of principal tides is less significant than that of higher harmonics within the estuary, the flood asymmetry is thus reduced after the TGD's operation. In contrast, the tidal duration asymmetry is enhanced at the downstream stations, where more complex morphological evolution occurs.

Discussion

Sensitivity of tidal amplitudes and phases to river discharge.
River discharge significantly influences tidal dynamics in the YRE, especially in the upper reaches[21,25,28,84], and can be described as a frequency-dependent modulation of the tidal amplitudes and phases[28,85]. NS_TIDE is used to conduct a sensitivity analysis for tidal amplitude and phase to different quantiles (0.8, 0.9, 1.0, 1.1 and 1.2) of the river discharge, and to evaluate the impact of river discharges on tidal motion in the YRE (Fig. 9).

Tidal amplitudes and phases respond to varying river discharge with a distinct spatial pattern. The two dominant diurnal tides (K_1 and O_1) are damped by increasing discharges in most parts of the YRE (Fig. 9a,b). Although relatively larger K_1 and O_1 tidal phases are found in the upper parts of the estuary at higher discharges, their tidal phases remain stable. The increasing K_1 amplitude downstream of Jiangyin is probably a result of increasing water depth from higher discharge, in accordance with the results of Matte et $al.$[74] in the lower reaches of the St. Lawrence fluvial estuary. Tidal amplitudes become more sharply damped by the river discharge upstream of Zhenjiang, indicating a separation of the estuary into tide- and river-dominated sections between Zhenjiang and Jiangyin, possibly due to breaks in the bed morphology[81] or rapid variation in bottom slope[74]. In contrast, O_1 seems less dependent on morphology, possibly due to different effects of M_2 on O_1 relative to K_1 under strong bottom frictions[86].

The dominant semidiurnal constituent (M_2) shows similar spatial variations as the diurnal constituents (K_1 and O_1) with respect to phases in most of the estuary (Fig. 9c). Slightly higher phases for M_2 occur at higher discharge, implying that tidal propagation is delayed under the increasing influence of river discharge. The amplitudes of M_2 decrease with increasing river discharge throughout the estuary, different from the two main diurnal constituents (K_1 and O_1) in the downstream region. At the upstream station (Wuhu), the M_2 amplitudes for the
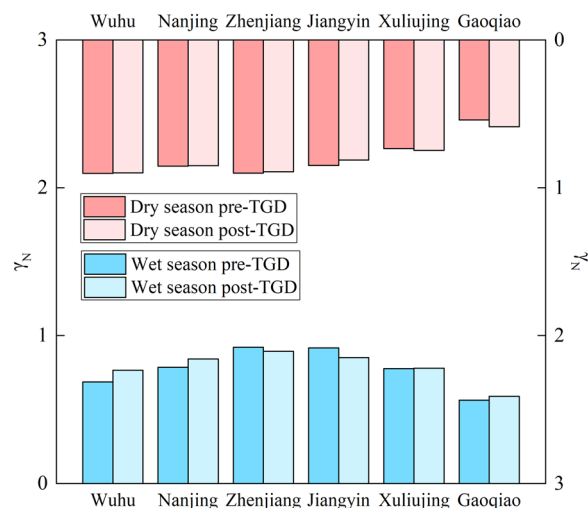
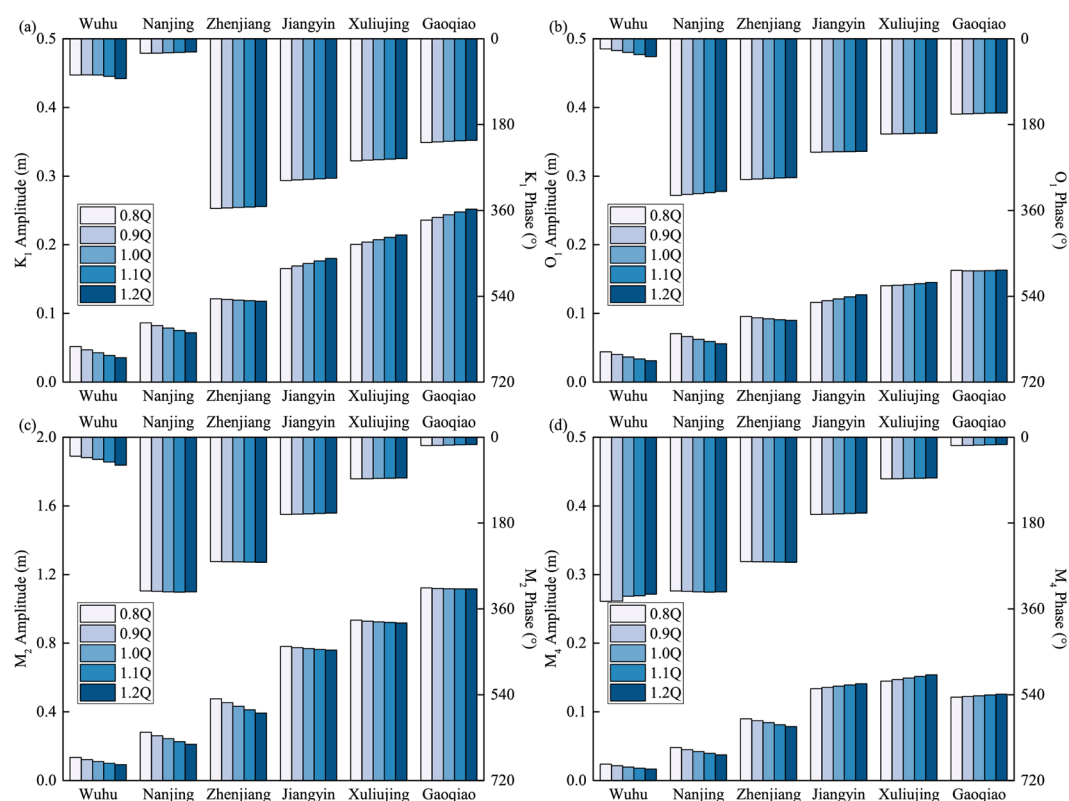**Figure 8.** Along-river variations in mean tidal skewness γ_N during the pre- and post-TGD periods.

Figure 9. Sensitivity of tidal amplitudes (bottom column) and phases (top column) to different quantiles of river discharge for (**a**) K_1, (**b**) O_1, (**c**) M_2 and (**d**) M_4.

0.8 quantiles of discharge (0.8Q) decrease by 31.3% at the 1.2 quantiles (1.2Q), whereas at the most seaward station (Gaoqiao) the decrease is only 0.5%, suggesting that varying river discharge barely modulates tidal amplitudes at the mouth of the estuary. This implies that the correlation in the upper reaches is more sensitive than that in the lower reaches.

The sensitivity of the quarter-diurnal tide (M_4) to river discharge to different quantiles of river discharge shows two clearly contrasting zones with marked changes in the M_4 amplitudes around Jiangyin and Zhenjiang (Fig. 9d). When the tide enters the estuary, the M_4 constituent is induced by friction, and its amplitude seems to be less sensitive to the varying discharge at Gaoqiao. As the tide propagates up the estuary, the increasing influence of discharge results in increasing M_4 amplitudes and lower M_4 phases at Xuliujing and Jiangyin, indicating an energy transfer from M_2 to M_4. Upstream of Jiangyin, M_4 is attenuated at higher discharges with smaller
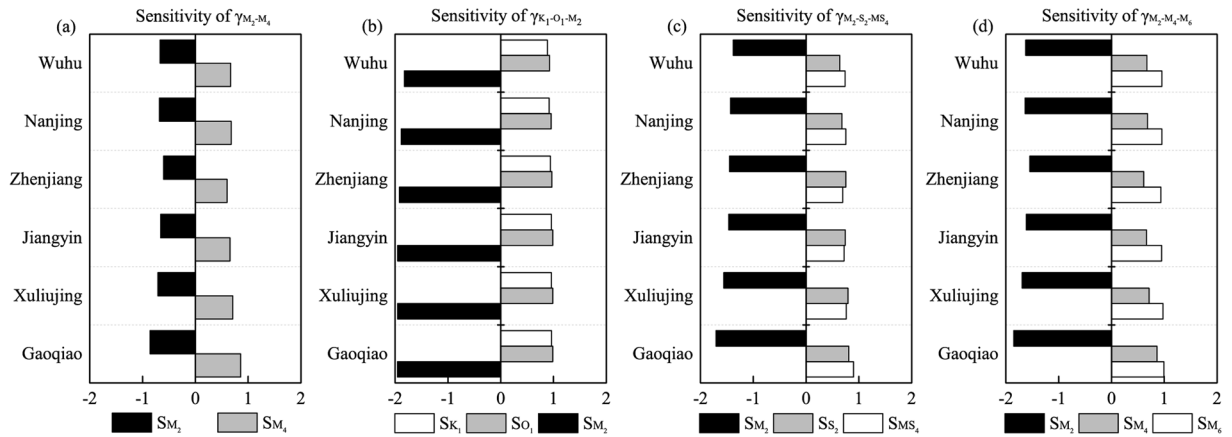
Figure 10. Mean value of relative sensitivity coefficients for different constituent amplitude variables contributing to tidal skewness at the six hydrological stations, generated by combinations of (**a**) M_2/M_4, (**b**) $K_1/O_1/M_2$, (**c**) $M_2/S_2/MS_4$ and (**d**) $M_2/M_4/M_6$.

amplitudes and larger phases along with the main tidal constituents. This spatially nonlinear behavior in response to varying discharge reveals the transition between tide- and river-dominated sections of the YRE.

Impacts of tidal attenuation and phase shifting on tidal duration asymmetry.   We perform a sensitivity analysis to quantify the response of the evolution of corresponding tidal amplitudes and phases to tidal skewness contributed by different combinations. The annual average relative sensitivity coefficients (RSCs) for the four major combinations (M_2/M_4, $K_1/O_1/M_2$, $M_2/S_2/MS_4$ and $M_2/M_4/M_6$) exhibit stable spatial patterns throughout the estuary (Fig. 10). The absolute RSC values of the dominant constituent M_2 and its first harmonic M_4 are equal, ranging from 0.60 to 0.86 (Fig. 10a). However, the effects of their evolutions on tidal duration asymmetry are not the same with regard to the sign. The M_2/M_4 asymmetry is enhanced by increasing M_4 and decreasing M_2 amplitudes in the downstream area, while being weakened as a result of the overall tidal damping in the upstream area, which reduces nonlinear behavior. Similar characteristics have been observed elsewhere in the world, such as in the Amazon Estuary[87], the Rhine-Meuse delta[88] and the St. Lawrence Fluvial Estuary[28,74].

Although astronomical tides gradually decay along the channel, their attenuation has different effects on tidal duration asymmetry. Regarding the sensitivity of the $K_1/O_1/M_2$ triad (Fig. 10b), the RSCs for the M_2 amplitude (S_{M_2}) show negative values ranging from -1.82 to -1.96, suggesting that tidal skewness ($\gamma_{K_1-O_1-M_2}$) may increase with the attenuation of the M_2 amplitude along the channel. In contrast, the positive values of S_{K_1} and S_{O_1} imply that the $K_1/O_1/M_2$ asymmetry may be reduced with a decrease in the amplitude of K_1 and O_1. As M_2 damps at a faster rate than K_1 and O_1, the reduction in the M_2 amplitude may result in a landward increase in the $K_1/O_1/M_2$ asymmetry.

The sensitivity coefficients for the M_2 amplitude (S_{M_2}) are also negative for $M_2/S_2/MS_4$ (Fig. 10c) and for $M_2/M_4/M_6$ (Fig. 10d), suggesting that the decay in the M_2 amplitude consistently enhances both the tidal duration asymmetry inherent in principal constituents and the asymmetry induced by nonlinearities in the YRE. Tidal duration asymmetry seems to be most sensitive to M_2 amplitude variation, because the RSCs for M_2 have the largest absolute values in each combination.

Phase differences can also play a crucial role in determining the direction of the tidal duration asymmetry[18,89], as large-scale tidal systems usually feature obvious variations in the tidal phase differences along the channel. The relative phase differences of the four combinations ($2\varphi_{M_2} - \varphi_{M_4}$, $\varphi_{K_1} + \varphi_{O_1} - \varphi_{M_2}$, $\varphi_{M_2} + \varphi_{S_2} - \varphi_{MS_4}$ and $\varphi_{M_2} + \varphi_{M_4} - \varphi_{M_6}$) assessed here are all below 180°, indicating flood-dominant asymmetry in the YRE (Fig. 11). The relative phase differences of the three combinations arising from nonlinearities ($2\varphi_{M_2} - \varphi_{M_4}$, $\varphi_{M_2} + \varphi_{S_2} - \varphi_{MS_4}$ and $\varphi_{M_2} + \varphi_{M_4} - \varphi_{M_6}$) experience slight modulations along the channel, except for a relatively sharp increase in $\varphi_{M_2} + \varphi_{M_4} - \varphi_{M_6}$ at Wuhu. This indicates that the impact of the spatial evolution of their tidal phase differences on the corresponding tidal duration asymmetry could be limited relative to attenuating tidal amplitudes. In contrast, the relative phase difference of the astronomical constituents ($\varphi_{K_1} + \varphi_{O_1} - \varphi_{M_2}$) significantly varies from 0° to 70° along the channel, especially in the upper reaches, in agreement with Guo et al.[41]. This could be another reason for the enhancement in tidal duration asymmetry of K_1-O_1-M_2 toward the upstream region.

Sensitivity of tidal duration asymmetry to river discharge.   The tidal skewness for different quantiles of discharge shows a nonlinear response (Fig. 12) with a comparatively high sensitivity of tidal skewness to river discharge in the upper reach. At the mouth of the estuary, the tidal duration asymmetry of M_2/M_4 is only slightly enhanced by the increasing river discharge, but this effect becomes more significant upstream, suggesting a nonlinear transfer of energy from M_2 to M_4 by friction, which is enhanced upstream under higher discharge conditions. In contrast, the correlation decreases in the middle segment of the YRE and the opposite holds upstream.
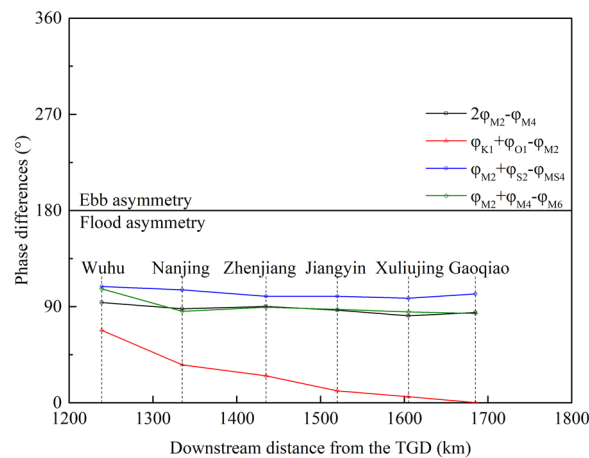
Figure 11. Along-channel variations in relative phase differences for four tidal combinations.

The flood asymmetry of M_2/M_4 is weakened with increasing discharge at Wuhu and Nanjing in the upper reaches. This matches the results of Guo et al.[23], who use the amplitude ratio D_4/D_2 to explore the response of tidal duration asymmetry to increased river discharge. Compared with the asymmetry of M_2/M_4, the flood asymmetry generated by astronomical tides ($K_1/O_1/M_2$) is far less sensitive to variations in discharge. In most of the estuary, only a slight reduction in the $K_1/O_1/M_2$ asymmetry is observed with increased river discharge (Fig. 12b). Controlled by interactions between river flow and tides, the tidal duration asymmetry induced by the combination of M_2-S_2-MS_4 and M_2-M_4-M_6 shows a similar spatial variation to M_2-M_4 (Fig. 12c,d). These responses of tidal duration asymmetry to river discharge can explain the variations in tidal skewness over the pre-TGD and post-TGD periods in the wet season (Fig. 8).

Impact of morphological changes on tidal duration asymmetry. The YRE has been seriously eroded since the operation of the TGD due to trapping of sediment behind the dam[27,43,90,91], with a total erosion volume of 2.157 billion m³. The average annual sediment discharge measured at Datong declines by 65% (from 4.43 Mt/yr to 1.51 Mt/yr) after the TGD's completion (Fig. 13). The TGD plays a dominant role in the reduction of sediment discharge at Datong, rather than the combined effects of other dams, precipitation and soil conservation. According to Zheng et al.[61], erosion rates have varied from 0.01 to 0.19 m per year along the channel. On average, the river reach has scoured approximately ~1.2 m (from −7 m to −8.2 m) in bed elevation after the completion of the TGD. As the increase in discharge is subtle in the dry season, morphological change rather than discharge regulation could be the dominant factor altering tidal duration asymmetry.

Morphological changes play an important role in the evolution of tidal duration asymmetry. A post-TGD increase in channel depth in the YRE could lead to a decrease in flood asymmetry during the dry season (Fig. 8), along with the modulation of tidal constituents. This is consistent with previous studies on tidal duration asymmetry suggesting that shallow tidal systems tend to be more flood-dominant than deeper systems[13,14,17,20,61,92].

Conclusions

A nonstationary harmonic analysis method is applied to examine the spatiotemporal evolution of tidal duration asymmetry under strongly variable river discharge conditions in the YRE, divided between the pre-TGD (1965–1985) and post-TGD (2003–2014) periods. The results quantify the contributions of dual and triad tidal combinations to the overall tidal duration asymmetries, based on tidal skewness. The hydrologic and morphologic effects are assessed based on the response of tidal duration asymmetry to varying river discharge and morphological changes, with the following main findings:

(1) The tidal duration asymmetry in the YRE is flood dominant. The interaction between M_2 and M_4 contribute mostly to the overall tidal duration asymmetry in the entire tidal system, followed by $M_2/S_2/MS_4$, $M_2/M_4/M_6$, and $K_1/O_1/M_2$. This indicates that tidal duration asymmetry within the YRE is significantly modulated by the effects of nonlinear interactions. Tidal duration asymmetry increases upstream, followed by a slight decrease, in accordance with the spatial pattern of tidal duration asymmetry induced by nonlinear effects (M_2/M_4, $M_2/S_2/MS_4$ and $M_2/M_4/M_6$), whereas tidal duration asymmetry induced by astronomical tides ($K_1/O_1/M_2$) consistently increases upstream. These results are related to the evolution of tidal amplitudes in terms of the non-dimensional relative sensitivity coefficients. In addition, phase shifts play an important role in affecting the evolution of the $K_1/O_1/M_2$ asymmetry in the upper reaches of the estuary, where the phase difference experiences obvious modulations.

(2) Tidal duration asymmetry varies significantly on a seasonal scale due to variations in river discharge. In the upper reaches, tidal duration asymmetry in the dry season is generally more significant than in the wet season, with the largest differences occurring furthest upstream. The opposite pattern is observed in the lower reaches, indicating that high river discharge in the wet season could accelerate energy transfer among tidal constituents. As a result, the generation of shallow-water constituents and the attenuation of astronomical constituents may lead to more asymmetric tides.
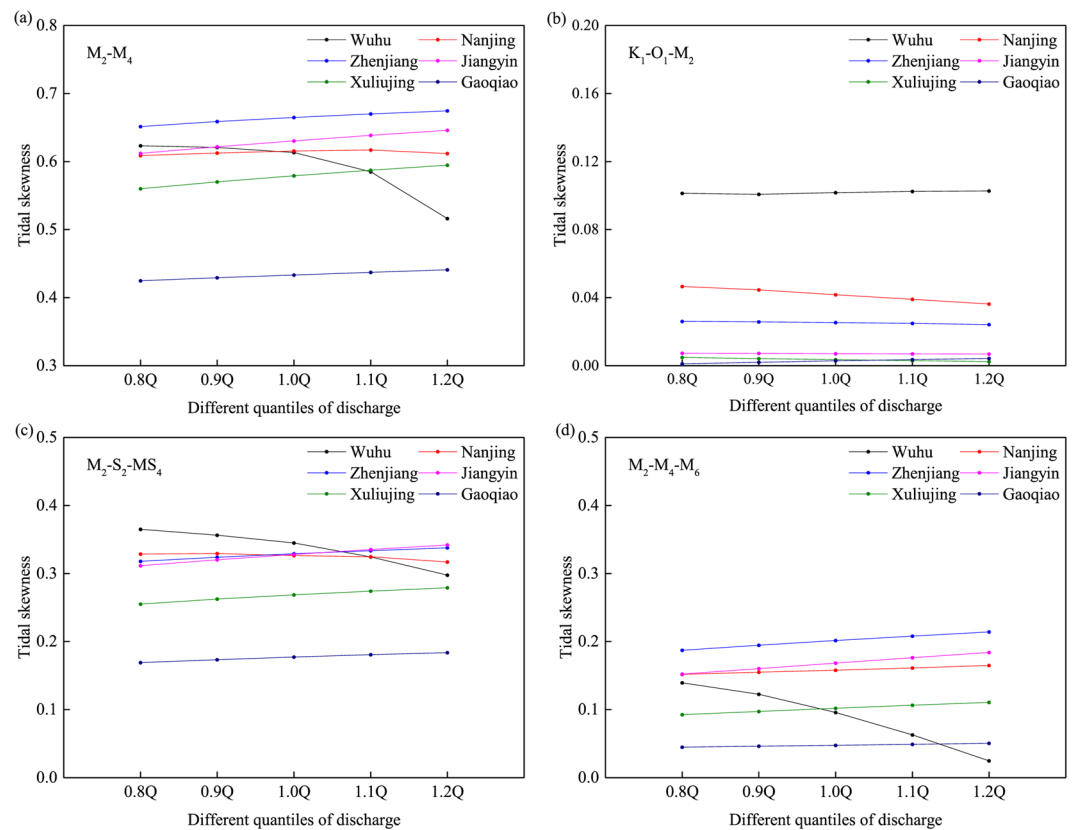
Figure 12. Tidal duration asymmetry for different quantiles of discharge induced by (**a**) M_2/M_4, (**b**) $K_1/O_1/M_2$, (**c**) $M_2/S_2/MS_4$ and (**d**) $M_2/M_4/M_6$.
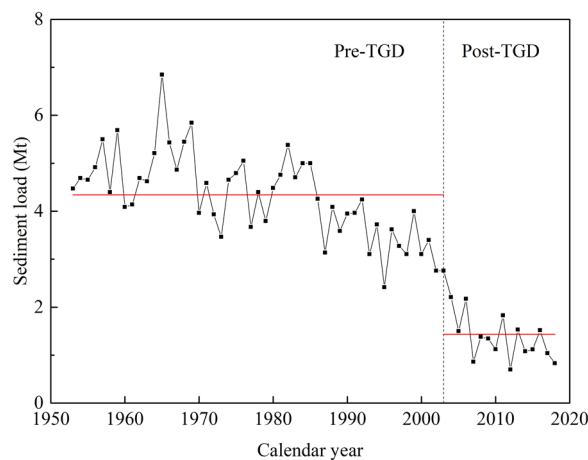

Figure 13. Annual sediment load for the YRE (measured at Datong). Red lines mark the average values for the pre-TGD (upper) and post-TGD (lower) periods.

(3) The TGD plays an important role in the discharge regulation and morphological changes in the YRE. Under the hydrologic and morphologic effects, tidal duration asymmetry experiences a seasonal modulation in the YRE. Changes in river discharge are significant at a seasonal scale. The regulation of the TGD and climate change impacts in the Yangtze basin can together explain the systematic changes in seasonality. The reduced river discharge in the wet season leads to an overall increase in tidal duration asymmetry upstream, whereas the reverse occurs downstream. In addition, sediment trapping mainly caused by the TGD produces morphological changes such as rapid erosion, thus deepening channel in the YRE. These effects become dominant (relative to discharge regulation) in the dry season when the discharge regulation is slight. The deepening channel reduces the flood asymmetry in most of the YRE.
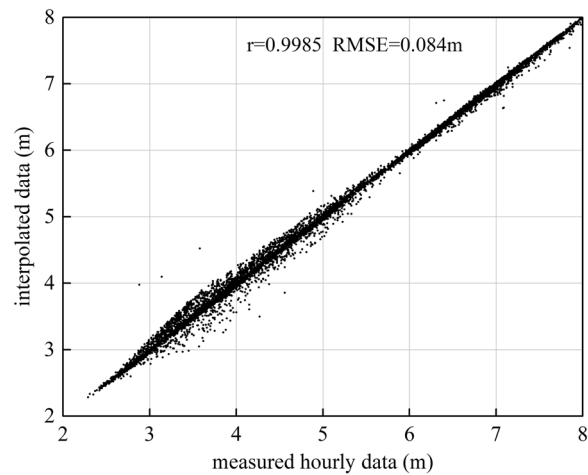
Figure A.1. Comparison between measured hourly data and the interpolated data at Nanjing station in 2014.
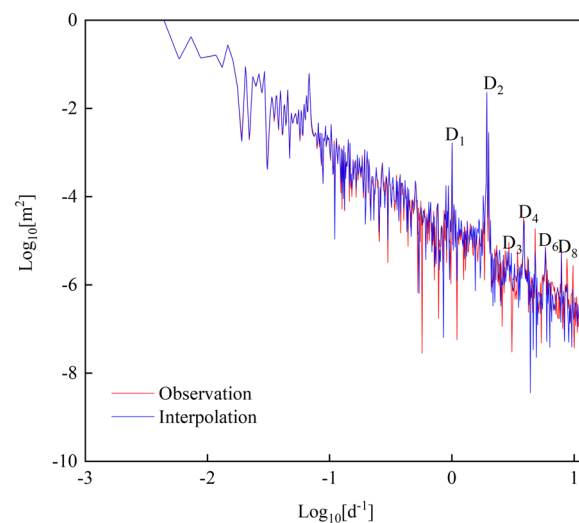

Figure A.2. Power spectrum for interpolated (blue line) and observed (red line) water levels at Nanjing in 2014.

Appendix A

Because of a lack of measured hourly data, trigonometrical interpolation is used to reconstruct hourly water levels based on high water-low water data. The performance of the interpolation method is here evaluated. The tidal height H(t) is modeled as:

$$H\left(t\right) = \frac{H_{n+1} + H_n}{2} - \frac{H_{n+1} - H_n}{2} \cos\left[\frac{\pi}{t_{n+1} - t_n}\left(t - t_n\right)\right]$$

where H_n and $H_n \pm 1$ refer to high water level and low water level respectively, t_n and $t_n \pm 1$ are the corresponding times.

The comparison between measured hourly data and the interpolated data at Nanjing in the period of 2014 is shown in Fig. A.1. The interpolated data fits well with the measured hourly data with the Pearson correlation coefficient (r) = 0.9985. Also, the root-mean-square error (RMSE) takes a value of 0.084 m, suggesting the interpolation is reliable.

The power spectrums of observations and interpolations are compared in Fig. A.2 based on a fast Fourier Transform (FFT). It shows that the frequency structure obtained by interpolation fits the observation well at D_1, D_2, D_4 and D_6, which are mainly focused in our study. Hence, the frequency structure obtained by trigonometrical interpolation performs well for the objective of this paper. Although the higher frequency band in the spectrum (including D_8 and higher harmonics) are not predicted well, the trigonometrical interpolation can reconstruct hourly water levels well for the purpose of our study. It's an effective tool for the analysis of low sampling frequency water levels when high and low water data are available only.

References

1. WCD (World Commission on Dams). Dams and development: a framework for decision making. (London, UK: Earthscan, 2000).
2. Chao, B. F., Wu, Y. H. & Li, Y. S. Impact of artificial reservoir water impoundment on global sea level. *Science* **320**, 212–214, https://doi.org/10.1126/science.1154580 (2008).
3. Graf, W. L. Downstream hydrologic and geomorphic effects of large dams on American rivers. *Geomorphology* **79**, 336–360, https://doi.org/10.1016/j.geomorph.2006.06.022 (2006).
4. Yang, S. L., Milliman, J. D., Li, P. & Xu, K. 50,000 dams later: Erosion of the Yangtze River and its delta. *Glob. Planet. Change* **75**, 14–20, https://doi.org/10.1016/j.gloplacha.2010.09.006 (2011).
5. Lehner, B. *et al*. High-resolution mapping of the world's reservoirs and dams for sustainable river-flow management. *Front. Ecol. Environ.* **9**, 494–502, https://doi.org/10.1890/100125 (2011).
6. Milliman, J. D. Oceanography - Blessed dams or damned dams? *Nature* **386**, 325–327, https://doi.org/10.1038/386325a0 (1997).
7. Nienhuis, J. H. *et al*. Global-scale human impact on delta morphology has led to net land area gain. *Nature* **577**, 514–518, https://doi.org/10.1038/s41586-019-1905-9 (2020).
8. Nienhuis, J. H., Hoitink, A. J. F. & Törnqvist, T. E. Future Change to Tide-Influenced Deltas. **45**, 3499–3507, https://doi.org/10.1029/2018gl077638 (2018).
9. Syvitski, J. P. M. *et al*. Sinking deltas due to human activities. *Nat. Geosci.* **2**, 681–686, https://doi.org/10.1038/Ngeo629 (2009).
10. Hoitink, A. J. F. & Jay, D. A. J. R. O. G. Tidal river dynamics: Implications for deltas. **54** (2016).
11. Hoitink, A. J. F., Wang, Z. B., Vermeulen, B., Huismans, Y. & Kästner, K. Tidal controls on river delta morphology. *Nat. Geosci.* **10**, 637–645, https://doi.org/10.1038/ngeo3000 (2017).
12. Boon, J. D. & Byrne, R. J. On basin hyposmetry and the morphodynamic response of coastal inlet systems. *Mar. Geol.* **40**, 27–48, https://doi.org/10.1016/0025-3227(81)90041-4 (1981).
13. Speer, P. E., Aubrey, D. G. & Friedrichs, C. T. In Tidal Hydrodynamics (ed. Parker, B. B.) 321–339 (John Wiley, Toronto, Ont., 1991).
14. Friedrichs, C. T. & Aubrey, D. G. Non-linear tidal distortion in shallow well-mixed estuaries: a synthesis. *Estuarine, Coast. Shelf Sci.* **27**, 521–545, https://doi.org/10.1016/0272-7714(88)90082-0 (1988).
15. Speer, P. E. & Aubrey, D. G. A study of non-linear tidal propagation in shallow inlet/estuarine systems Part II: Theory. *Estuarine, Coast. Shelf Sci.* **21**, 207–224, https://doi.org/10.1016/0272-7714(85)90097-6 (1985).
16. Gong, W. P., Schuttelaars, H. & Zhang, H. Tidal asymmetry in a funnel-shaped estuary with mixed semidiurnal tides. *Ocean. Dynam* **66**, 637–658, https://doi.org/10.1007/s10236-016-0943-1 (2016).
17. Dronkers, J. Tidal asymmetry and estuarine morphology. *Neth. J. Sea Res.* **20**, 117–131, https://doi.org/10.1016/0077-7579(86)90036-0 (1986).
18. Hoitink, A. J. F., Hoekstra, P. & van Maren, D. S. Flow asymmetry associated with astronomical tides: Implications for the residual transport of sediment. *J Geophys Res-Oceans* **108**, https://doi.org/10.1029/2002jc001539 (2003).
19. Woodworth, P. L., Blackman, D. L., Pugh, D. T. & Vassie, J. M. On the role of diurnal tides in contributing to asymmetries in tidal probability distribution functions in areas of predominantly semi-diurnal tide. *Estuar. Coast. Shelf S* **64**, 235–240, https://doi.org/10.1016/j.ecss.2005.02.014 (2005).
20. Friedrichs, C. T. & Madsen, O. S. Nonlinear diffusion of the tidal signal in frictionally dominated embayments. *Journal of Geophysical Research* **97**, https://doi.org/10.1029/92jc00354 (1992).
21. Jay, D. A. Green's law revisited: Tidal long-wave propagation in channels with strong topography. *J. Geophys. Res.* **96**, 20585–20598, https://doi.org/10.1029/91jc01633 (1991).
22. Guo, L. *et al*. River-tide dynamics: Exploration of nonstationary and nonlinear tidal behavior in the Yangtze River estuary. *J. Geophys. Res-Oceans* **120**, 3499–3521, https://doi.org/10.1002/2014jc010491 (2015).
23. Flinchem, E. P. & Jay, D. A. An introduction to wavelet transform tidal analysis methods. *Estuar. Coast. Shelf S* **51**, 177–200, https://doi.org/10.1006/ecss.2000.0586 (2000).
24. Jay, D. A. & Kukulka, T. Revising the paradigm of tidal analysis- the uses of non-stationary data. *Ocean. Dynam* **53**, 110–125, https://doi.org/10.1007/s10236-003-0042-y (2003).
25. Godin, G. Modification of River Tides by the Discharge. *J. Waterway, Port, Coastal, Ocean. Eng.* **111**, 257–274, https://doi.org/10.1061/(asce)0733-950x(1985)111:2(257) (1985).
26. Cai, H. Y., Savenije, H. H. G., Yang, Q. S., Ou, S. Y. & Lei, Y. P. Influence of River Discharge and Dredging on Tidal Wave Propagation: Modaomen Estuary Case. *J. Hydraul. Eng.* **138**, 885–896, https://doi.org/10.1061/(Asce)Hy.1943-7900.0000594 (2012).
27. Godin, G. Frictional effects in river tides. *Tidal hydrodynamics* **379**, 402 (1991).
28. Godin, G. The propagation of tides up rivers with special considerations on the upper Saint Lawrence river. *Estuar. Coast. Shelf S* **48**, 307–324, https://doi.org/10.1006/ecss.1998.0422 (1999).
29. LeBlond, P. H. On tidal propagation in shallow rivers. *J. Geophys. Res.* **83**, 4717–4721, https://doi.org/10.1029/JC083iC09p04717 (1978).
30. Lincoln, J. M. & Fitzgerald, D. M. Tidal distortions and flood dominance at five small tidal inlets in southern Maine. **82**, 133-148.
31. Nidzieko, N. J. Tidal asymmetry in estuaries with mixed semidiurnal/diurnal tides. *J Geophys Res-Oceans* **115**, https://doi.org/10.1029/2009jc005864 (2010).
32. Van de Kreeke, J. & Robaczewska, K. Tide-induced residual transport of coarse sediment; Application to the EMS estuary. *Neth. J. Sea Res.* **31**, 209–220, https://doi.org/10.1016/0077-7579(93)90022-k (1993).
33. van Maren, D. S. & Winterwerp, J. C. The role of flow asymmetry and mud properties on tidal flat sedimentation. *Cont. Shelf Res.* **60**, S71–S84 (2013).
34. Wang, Z., Jeuken, C. & De Vriend, H. Tidal asymmetry and residual sediment transport in estuaries. *Delft Hydraulics report Z2749* (1999).
35. Aubrey, D. G. & Speer, P. E. A study of non-linear tidal propagation in shallow inlet/estuarine systems Part I: Observations. *Estuarine, Coast. Shelf Sci.* **21**, 185–205, https://doi.org/10.1016/0272-7714(85)90096-4 (1985).
36. Song, D. H., Wang, X. H., Kiss, A. E. & Bao, X. W. The contribution to tidal asymmetry by different combinations of tidal constituents. *J Geophys Res-Oceans* **116**, https://doi.org/10.1029/2011jc007270 (2011).
37. Zhang, E. F., Savenije, H. H. G., Chen, S. L. & Mao, X. H. An analytical solution for tidal propagation in the Yangtze Estuary, China. *Hydrol. Earth Syst. Sc.* **16**, 3327–3339, https://doi.org/10.5194/hess-16-3327-2012 (2012).
38. Lu, S. *et al*. Propagation of tidal waves up in Yangtze Estuary during the dry season. *J. Geophys. Res-Oceans* **120**, 6445–6473, https://doi.org/10.1002/2014jc010414 (2015).
39. Alebregtse, N. C. & de Swart, H. E. Effect of river discharge and geometry on tides and net water transport in an estuarine network, an idealized model applied to the Yangtze Estuary. *Cont. Shelf Res.* **123**, 29–49, https://doi.org/10.1016/j.csr.2016.003.028 (2016).
40. Cai, H., Savenije, H. H. G. & Toffolon, M. Linking the river to the estuary: influence of river discharge on tidal damping. *Hydrol. Earth Syst. Sc.* **18**, 287–304, https://doi.org/10.5194/hess-18-287-2014 (2014).
41. Guo, L. C., van der Wegen, M., Wang, Z. B., Roelvink, D. & He, Q. Exploring the impacts of multiple tidal constituents and varying river flow on long-term, large-scale estuarine morphodynamics by means of a 1-D model. *J. Geophys. Res-Earth* **121**, 1000–1022, https://doi.org/10.1002/2016jf003821 (2016).

42. Kuang, C. P. *et al*. River discharge contribution to sea-level rise in the Yangtze River Estuary, China. *Cont. Shelf Res.* **134**, 63–75, https://doi.org/10.1016/j.csr.2017.01.004 (2017).
43. Luan, H. L., Ding, P. X., Wang, Z. B., Ge, J. Z. & Yang, S. L. Decadal morphological evolution of the Yangtze Estuary in response to river input changes and estuarine engineering projects. *Geomorphology* **265**, 12–23, https://doi.org/10.1016/j.geomorph.2016.04.022 (2016).
44. Zhang, M., Townend, I. H., Cai, H. Y. & Zhou, Y. X. Seasonal variation of tidal prism and energy in the Changjiang River estuary: a numerical study. *Chin. J. Oceanol. Limn.* **34**, 219–230, https://doi.org/10.1007/s00343-015-4302-8 (2016).
45. Shen, G. & Xie, Z. Three Gorges project: chance and challenge. *Science* **304**, 681, https://doi.org/10.1126/science.304.5671.681b (2004).
46. Dai, Z., Liu, J. T., Wei, W. & Chen, J. Detection of the Three Gorges Dam influence on the Changjiang (Yangtze River) submerged delta. *Sci. Rep-Uk* **4**, 6600, https://doi.org/10.1038/srep06600 (2014).
47. Xu, K., Milliman, J. D., Yang, Z. & Wang, H. Yangtze sediment decline partly from Three Gorges Dam. *Eos, Trans. Am. Geophys. Union.* **87**, 185–190, https://doi.org/10.1029/2006eo190001 (2006).
48. Yang, S. L. *et al*. Temporal variations in water resources in the Yangtze River (Changjiang) over the Industrial Period based on reconstruction of missing monthly discharges. *Water Resour Res* **46** (2010).
49. Mei, X. F. *et al*. Modulation of Extreme Flood Levels by Impoundment Significantly Offset by Floodplain Loss Downstream of the Three Gorges Dam. *Geophys. Res. Lett.* **45**, 3147–3155 (2018).
50. Yang, S. L. *et al*. Downstream sedimentary and geomorphic impacts of the Three Gorges Dam on the Yangtze River. *Earth-Sci Rev.* **138**, 469–486 (2014).
51. Yang, H. F. *et al*. Human impacts on sediment in the Yangtze River: A review and new perspectives. *Glob. Planet. Change* **162**, 8–17 (2018).
52. Yang, S. L., Zhang, J. & Xu, X. J. Influence of the Three Gorges Dam on downstream delivery of sediment and its environmental implications, Yangtze River. *Geophys Res Lett* **34** (2007).
53. Li, P. *et al*. Spatial, Temporal, and Human-Induced Variations in Suspended Sediment Concentration in the Surface Waters of the Yangtze Estuary and Adjacent Coastal Areas. *Estuar. Coast.* **35**, 1316–1327 (2012).
54. Du, J. L., Yang, S. L. & Feng, H. Recent human impacts on the morphological evolution of the Yangtze River delta foreland: A review and new perspectives. *Estuar. Coast. Shelf S* **181**, 160–169 (2016).
55. Yang, H. F. *et al*. Erosion potential of the Yangtze Delta under sediment starvation and climate change. *Scientific Reports* **7** (2017).
56. Luo, X. X., Yang, S. L. & Zhang, J. The impact of the Three Gorges Dam on the downstream distribution and texture of sediments along the middle and lower Yangtze River (Changjiang) and its estuary, and subsequent sediment dispersal in the East China Sea. *Geomorphology* **179**, 126–140, https://doi.org/10.1016/j.geomorph.2012.05.034 (2012).
57. Luo, X. X., Yang, S. L., Wang, R. S., Zhang, C. Y. & Li, P. New evidence of Yangtze delta recession after closing of the Three Gorges Dam. *Sci. Rep-Uk* **7**, 41735, https://doi.org/10.1038/srep41735 (2017).
58. Yang, H. F. *et al*. Recent coarsening of sediments on the southern Yangtze subaqueous delta front: A response to river damming. *Cont. Shelf Res.* **155**, 45–51 (2018).
59. Xu, K., Milliman, J. D., Yang, Z. & Xu, H. In Large Rivers: Geomorphology and Management (John Wiley & Sons, Ltd, 2008).
60. Yang, S. L. *et al*. Effects of human activities on the Yangtze River suspended sediment flux into the estuary in the last century. *Hydrol. Earth Syst. Sc.* **8**, 1210–1216 (2004).
61. Zheng, S. *et al*. Riverbed erosion of the final 565 kilometers of the Yangtze River (Changjiang) following construction of the Three Gorges Dam. *Sci. Rep-Uk* **8**, 11917, https://doi.org/10.1038/s41598-018-30441-6 (2018).
62. Zhang, F. Y., Sun, J., Lin, B. L. & Huang, G. X. Seasonal hydrodynamic interactions between tidal waves and river flows in the Yangtze Estuary. *J. Mar. Syst.* **186**, 17–28, https://doi.org/10.1016/j.jmarsys.2018.05.005 (2018).
63. Cai, H. *et al*. Impacts of Three Gorges Dam's operation on spatial-temporal patterns of tide-river dynamics in the Yangtze River estuary, China. *Ocean. Sci.* **15**, 583–599, https://doi.org/10.5194/os-15-583-2019 (2019).
64. Chen, Z. Y., Wang, Z. H., Finlayson, B., Chen, J. & Yin, D. W. Implications of flow control by the Three Gorges Dam on sediment and channel dynamics of the middle Yangtze (Changjiang) River, China. *Geology* **38**, 1043–1046, https://doi.org/10.1130/G31271.1 (2010).
65. Lai, X. *et al*. Will river erosion below the Three Gorges Dam stop in the middle Yangtze? *J. Hydrol.* **554**, 24–31, https://doi.org/10.1016/j.jhydrol.2017.08.057 (2017).
66. Yun, C. X. *Recent Evolution of the Yangtze Estuary and Its Mechanisms [in Chinese]*. (China Ocean Press,Beijing, 2004).
67. Wang, W. P., Zhu, Y. L., Dong, S. F., Becker, S. & Chen, Y. F. Attribution of decreasing annual and autumn inflows to the Three Gorges Reservoir, Yangtze River: Climate variability, water consumption or upstream reservoir operation? *J Hydrol* **579** (2019).
68. Chai, Y. *et al*. Influence of Climate Variability and Reservoir Operation on Streamflow in the Yangtze River. *Scientific Reports* **9** (2019).
69. Doodson, A. T. The harmonic development of the tide-generating potential. *Proc. R. Soc. London. Ser. A, Containing Pap. a Math. Phys. Character* **100**, 305–329 (1921).
70. Darwin, G. H. On an Apparatus for Facilitating the Reduction of Tidal Observations. *Proc.roy.soc.london Ser.a* **52**, 345–389 (1892).
71. Jay, D. A. & Flinchem, E. P. A comparison of methods for analysis of tidal records containing multi-scale non-tidal background energy. *Cont. Shelf Res.* **19**, 1695–1732 (1999).
72. Pawlowicz, R., Beardsley, B. & Lentz, S. Classical tidal harmonic analysis including error estimates in MATLAB using T-TIDE. *Comput. Geosci-Uk* **28**, 929–937 (2002).
73. Matte, P., Jay, D. A. & Zaron, E. D. Adaptation of Classical Tidal Harmonic Analysis to Nonstationary Tides, with Application to River Tides. *J. Atmos. Ocean. Tech.* **30**, 569–589, https://doi.org/10.1175/Jtech-D-12-00016.1 (2013).
74. Matte, P., Secretan, Y. & Morin, J. Temporal and spatial variability of tidal-fluvial dynamics in the St. Lawrence fluvial estuary: An application of nonstationary tidal harmonic analysis. *J. Geophys. Res-Oceans* **119**, 5724–5744, https://doi.org/10.1002/2014jc009791 (2014).
75. McCuen, R. H. A Sensitivity and Error Analysis Cf Procedures Used for Estimating Evaporation. *J. Am. Water Resour. Assoc.* **10**, 486–497, https://doi.org/10.1111/j.1752-1688.1974.tb00590.x (1974).
76. Pugh, D. Changing Sea Levels - Effects of Tides, Weather and Climate. *Changing Sea Levels Effects of Tides Weather & Climate*, **280**, https://doi.org/10.1007/1-4020-3880-1_66 (2004).
77. Defant, A. *Physical oceanography*. Vol. 1 (Pergamon, 1961).
78. Guo, L. C., Brand, M., Sanders, B. F., Foufoula-Georgiou, E. & Stein, E. D. Tidal asymmetry and residual sediment transport in a short tidal basin under sea level rise. *Adv. Water Resour.* **121**, 1–8, https://doi.org/10.1016/j.advwatres.2018.07.012 (2018).
79. Buschman, F. A., Hoitink, A. J. F., van der Vegt, M. & Hoekstra, P. Subtidal water level variation controlled by river flow and tides. *Water Resour Res* **45**, https://doi.org/10.1029/2009wr008167 (2009).
80. Sassi, M. G. & Hoitink, A. J. F. River flow controls on tides and tide-mean water level profiles in a tidal freshwater river. *J. Geophys. Res-Oceans* **118**, 4139–4151, https://doi.org/10.1002/jgrc.20297 (2013).
81. Sassi, M. G., Hoitink, A. J. F., de Brye, B. & Deleersnijder, E. Downstream hydraulic geometry of a tidally influenced river delta. *J Geophys Res-Earth* **117**, https://doi.org/10.1029/2012JF002448 (2012).
82. Zhang, W., Feng, H., Zhu, Y. & Hoitink, A. J. F. Subtidal flow reversal associated with sediment accretion in a delta channel. *Water Resour Res* **55**, https://doi.org/10.1029/2019WR025945 (2019).

83. Winterwerp, J. C. Fine sediment transport by tidal asymmetry in the high-concentrated Ems River: indications for a regime shift in response to channel deepening. *Ocean. Dynam* **61**, 203–215, https://doi.org/10.1007/s10236-010-0332-0 (2011).

84. Jay, D. A. & Flinchem, E. P. Interaction of fluctuating river flow with a barotropic tide: A demonstration of wavelet tidal analysis methods. *J. Geophys. Res-Oceans* **102**, 5705–5720, https://doi.org/10.1029/96jc00496 (1997).

85. Horrevoets, A. C., Savenije, H. H. G., Schuurman, J. N. & Graas, S. The, influence of river discharge on tidal damping in alluvial estuaries. *J. Hydrol.* **294**, 213–228, https://doi.org/10.1016/j.jhydrol.2004.02.012 (2004).

86. Godin, G. & Martínez, A. Numerical experiments to investigate the effects of quadratic friction on the propagation of tides in a channel. *Cont. Shelf Res.* **14**, 723–748, https://doi.org/10.1016/0278-4343(94)90070-1 (1994).

87. Gallo, M. N. & Vinzon, S. B. Generation of overtides and compound tides in Amazon estuary. *Ocean. Dynam* **55**, 441–448, https://doi.org/10.1007/s10236-005-0003-8 (2005).

88. Vellinga, N. E., Hoitink, A. J. F., van der Vegt, M., Zhang, W. & Hoekstra, P. Human impacts on tides overwhelm the effect of sea level rise on extreme water levels in the Rhine-Meuse delta. *Coast. Eng.* **90**, 40–50, https://doi.org/10.1016/j.coastaleng.2014.04.005 (2014).

89. Guo, L., van der Wegen, M., Roelvink, J. A. & He, Q. The role of river flow and tidal asymmetry on 1-D estuarine morphodynamics. *J. Geophys. Res-Earth* **119**, 2315–2334, https://doi.org/10.1002/2014jf003110 (2014).

90. Jiang, C. J., Li, J. F. & de Swart, H. E. Effects of navigational works on morphological changes in the bar area of the Yangtze Estuary. *Geomorphology* **139**, 205–219, https://doi.org/10.1016/j.geomorph.2011.10.020 (2012).

91. Wu, S. H., Cheng, H. Q., Xu, Y. J., Li, J. F. & Zheng, S. W. Decadal changes in bathymetry of the Yangtze River Estuary: Human impacts and potential saltwater intrusion. *Estuar. Coast. Shelf S* **182**, 158–169, https://doi.org/10.1016/j.ecss.2016.10.002 (2016).

92. Wang, Z. B., Jeuken, M. C. J. L., Gerritsen, H., de Vriend, H. J. & Kornman, B. A. Morphology and asymmetry of the vertical tide in the Westerschelde estuary. *Cont. Shelf Res.* **22**, 2599–2609, https://doi.org/10.1016/S0278-4343(02)00134-6 (2002).

Acknowledgements

Author contributions

Xiayan Yu, Wei Zhang and A.J.F. Hoitink jointly conducted the study. Wei Zhang developed the idea for the study and performed the supervision. Wei Zhang and Xiayan Yu carried out the data analysis. Xiayan Yu wrote the main part of the manuscript. A.J.F. Hoitink refined the ideas and participated in the revision of manuscript. All authors read and approved the final manuscript.

Competing interests

The authors declare no competing interests.

Additional information

Correspondence and requests for materials should be addressed to W.Z.

Reprints and permissions information is available at www.nature.com/reprints.

Publisher's note Springer Nature remains neutral with regard to jurisdictional claims in published maps and institutional affiliations.